Experimental validation of an eddy current probe for defect detection in thick conducting specimen

Cite as: AIP Conference Proceedings **1706**, 020025 (2016); https://doi.org/10.1063/1.4940471
Published Online: 10 February 2016

Mahesh Raja P., Kavitha Arunachalam, and Krishnan Balasubramanian

Experimental Validation of an Eddy Current Probe for Defect Detection in Thick Conducting Specimen

Mahesh Raja P[1a)], Kavitha Arunachalam[2b)], Krishnan Balasubramanian[3c)]

[1, 2]*Electromagnetic Research Laboratory, Department of Engineering Design, Indian Institute of Technology Madras, Chennai*
[3]*Centre for Non-Destructive Evaluation (CNDE), Department of Mechanical Engineering Indian Institute of Technology Madras, Chennai, Tamil Nadu, India-600036*

[a)] *mrp0559@gmail.com*
[b)] *akavitha@iitm.ac.in*
[c)]*balas@iitm.ac.in*

Abstract: This paper presents numerical modeling and experimental measurements of eddy current (EC) probe for detecting subsurface defects in 10 mm to 15 mm thick conducting specimen. Measurements are presented for a pancake air core coil to detect subsurface defect in 10 mm thick aluminum slab. EC coil parameters namely inner radius(r_1), and outer radius(r_2), and operating frequency (f) are optimized for deeper penetration in the conducting plate (35 MS/m) for a given coil height(h), and lift off distance (d). Preliminary simulation results are presented for a subsurface defect in 15 mm thick aluminium plate for the optimized EC coil parameters.

INTRODUCTION

Eddy current testing (ECT) is one of the commonly used nondestructive testing (NDT) techniques for inspecting electrically conducting materials. It works on the principle of electromagnetic (EM) induction, where a coil carrying alternating current (AC) induces eddy current when it is brought near a conducting specimen. Flow of eddy current is locally perturbed in the presence of cracks/defects which change the associated secondary magnetic field and the coil impedance. The change in coil impedance is used for detection and characterization of the damage. The eddy current induced in the specimen is concentrated primarily on the surface close to the coil and attenuates along the depth of the sample due to skin depth phenomenon [1]. Skin depth, δ is also inversely proportional to the coil excitation frequency and electrical conductivity of the sample. Thus, ECT is widely used for defect detection in thinner conducting specimen typically, 3 mm – 6 mm thickness. In this paper, we present EC coil measurements for a subsurface defect in a 10 mm aluminum sample. 3D numerical modeling is used for optimization of the air core coil and operating frequency. Simulations for the optimized ECT parameters indicate measurable change in coil impedance for a subsurface defect in 15 mm thick aluminum plate.

EC COIL EXPERIMENTS

Figure 1 shows an illustration of a pancake coil above a conducting specimen with centrally located two dimensional (2D) subsurface defect. The conducting specimen is a 10 mm thick aluminium slab of length, 100 mm and width, 30 mm. A 0.5 mm wide 2D notch of 1 mm depth on the far side of the coil was scanned using an air core pancake coil connected to a LCR meter. The coil parameters used in the experiment are as follows: inner diameter

42nd Annual Review of Progress in Quantitative Nondestructive Evaluation
AIP Conf. Proc. 1706, 020025-1–020025-5; doi: 10.1063/1.4940471

(ID), D_1 = 4 mm, outer diameter (OD), D_2=18 mm, height, h= 3 mm, number of turns, N= 525 and wire gauge, 38. The coil inductance, L in air and above the sample is 2.73 mH and 2.33 mH respectively. The skin depth (δ) of the coil in the sample is 2.9 mm at 1 kHz.

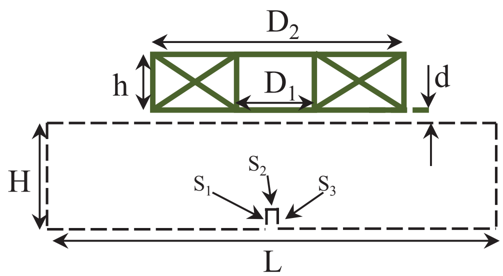

FIGURE 1. Coil and sample geometry showing defect surfaces S_1, S_2, and S_3.

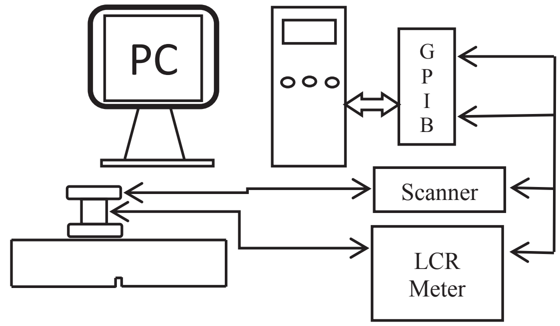

FIGURE 2. Experimental Setup

Figure 2 shows the experimental setup for coil impedance measurements. Coil excitation was given through an impedance analyzer (E4980A, Agilent Technologies, USA) which produces a sinusoidal signal with 20 mA current. Coil lift off was maintained as 1 mm using a computer controlled 2D scanner. The coil was scanned above the sample in steps of 1 mm with the help of a scanner controlled via a custom LABVIEW program. At each scan position, coil impedance, $Z = R + jX$ was recorded at three frequencies namely, 250 Hz, 350 Hz and 450 Hz for the deep seated defect. Normalized coil resistance, $R_n = (R - R_0)/X_0$ and reactance, $X_n = X/X_0$ where R_0 is coil resistance, X_0 is coil reactance in air and $X = 2\pi fL$.

Figure 3 shows the impedance plane trajectory as the coil was scanned above the sample. It can be seen from Fig. 3a that the magnitude of coil impedance varies with frequency. The lowest frequency shows the largest change than higher frequencies. The pancake air core coil was used to measure subsurface notch in a 15 mm thick aluminium plate. The coil sensitivity for the subsurface defect was poor due to decreased eddy current density [2]. Hence, coil parameters and excitation frequencies were optimized using 3D numerical simulations.

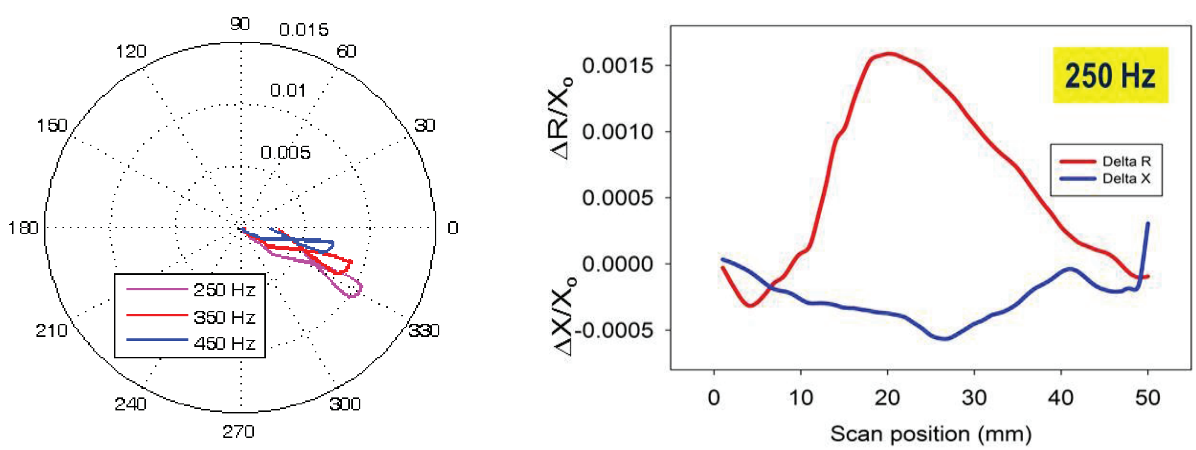

(a) (b)

FIGURE 3. (a) Coil impedance plane trajectory for a sub-surface notch located 9 mm deep in 10 mm thick aluminium plate. (b) Change in normalized coil impedance at 250 Hz. Defect depth is 1 mm.

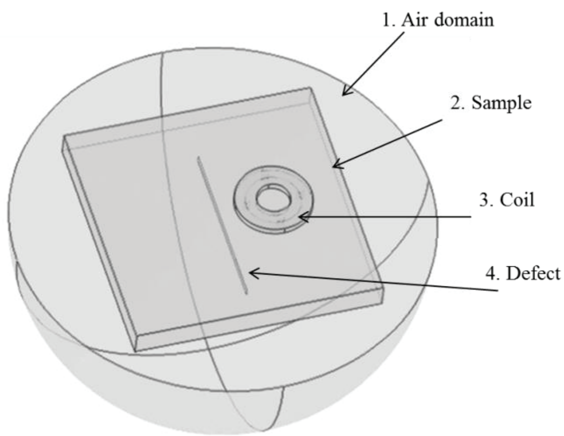

FIGURE 4. Schematic of the FEM model

NUMERICAL MODELING FOR COIL OPTIMIZATION

Numerical simulations for coil optimization were carried out using Finite Element Method (FEM) based simulation software, COMSOL Multiphysics®. Modeling practice reported in literature for solving ECT problems was adopted in our work [3]. The mathematical formulation for the numerical model is given by Maxwell's equation together with constitutive equations and ohm's law. Figure 4 shows the 3D model developed in COMSOL for coil optimization. The simplified form of the governing equation [4],

$$\nabla^2 \boldsymbol{A} = -\mu i_0 + \mu\sigma\left(\frac{\partial \boldsymbol{A}}{\partial t}\right) + \mu\epsilon\left(\frac{\partial^2 \boldsymbol{A}}{\partial t^2}\right) + \mu\nabla\left(\frac{1}{\mu}\right) \times (\nabla \times \boldsymbol{A}), \quad (1)$$

is applicable to all sub domains in the computational model. In Eqn. (1), $\mathbf{A}$ is magnetic vector potential, σ is electrical conductivity (S/m), μ is magnetic permeability (H/m) and i_0 is coil current (mA). External boundary of the air domain was subjected to magnetic insulation, $\hat{n} \times \boldsymbol{A} = 0$ where $\hat{n}$ denotes the outward unit surface normal. Coil excitation was assigned by applying a uniform vector current density J_o to the coil. Simulation results were validated with benchmark problems provided by the World Federation of Nondestructive Evaluation Centers.

SIMULATIONS

Simulations were carried out to determine coil inner and outer radii $(\mathrm{r}_1, \mathrm{r}_2)$, and optimal operating frequency for fixed coil height $(\mathrm{h} = 3\ \mathrm{mm})$, number of turns $(\mathrm{N} = 200)$ and 0.1 mm lift off above a 15 mm thick aluminium plate. A 4.5 mm deep 2D notch of width 0.5 mm was positioned on the bottom of the plate. The plate electrical conductivity (σ) and relative permeability (μ_r) was assigned as 35 MS/m and 1 respectively. The plate dimensions were 150 mm × 150 mm. The average magnetic field density, $(\mathbf{B} = \nabla \times \mathbf{A})$ induced by the air core coil on the notch surface, S_2 was calculated for varying coil radii as the excitation frequency was swept from 40 Hz till 500 Hz.

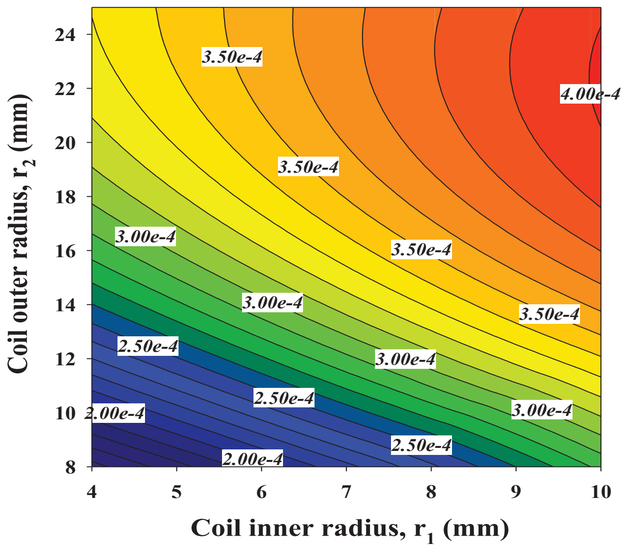

(a)

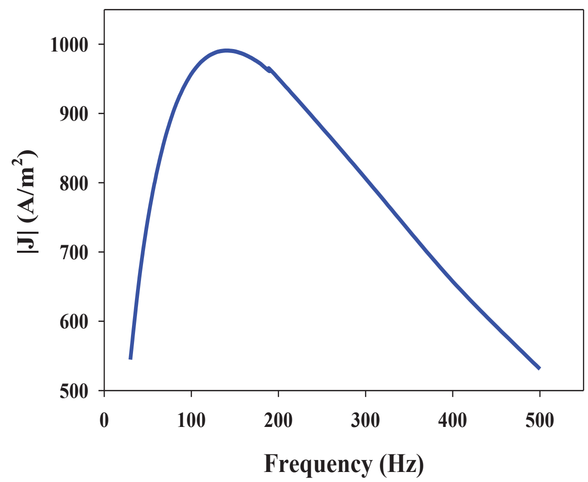

(b)

FIGURE 5. (a) Magnitude of magnetic field density, $|\boldsymbol{B}|$ at 150 Hz on the defect surface (S_2) for varying coil inner (r_1) and outer (r_2) radii, (r_1: 4 mm to 10 mm; r_2: 8 mm to 25 mm); (b) induced current density at plate bottom for r_1 = 10 mm, r_2 = 23 mm, *h*= 3 mm, *d*=0.5 mm.

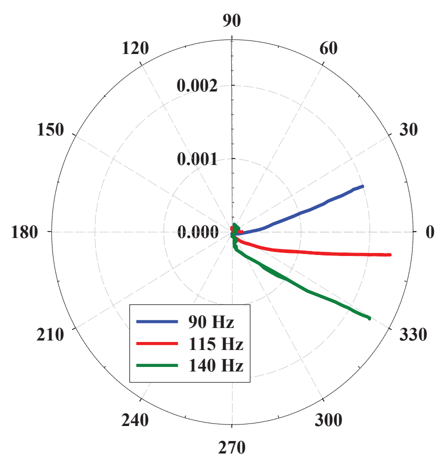

FIGURE 6. Impedance plane trajectory of optimized EC coil for 11.5 mm deep 2D notch in 15 mm thick aluminium plate**.**

Figure 5a shows the magnitude of the magnetic field density ($|\boldsymbol{B}|$) on the notch surface (S_2) as indicated in Fig. 1 for varying coil inner and outer radii at 150 Hz. It can be seen from the contour plot that the magnetic field density is maximum for coil inner and outer radius of 10 mm and 23 mm respectively. The optimum excitation frequency for these coil parameters was found by calculating the magnitude of the induced current density at the bottom of plate [5]. Figure 5b shows the induced current as a function of excitation frequency for coil inner and outer radii of 10 mm and 23 mm respectively. In Fig. 5b the current density induced at the bottom of the plate reaches maximum at 140 Hz. Subsequently simulations were carried out at the optimized excitation frequency for the chosen coil parameters as the coil was scanned above an 11.5 mm deep subsurface 2D notch of width, 0.5 mm in a 15 mm thick aluminium plate. Figure 6 shows the simulated impedance plane trajectory for the 2D notch centered in the 15 mm thick aluminium plate. Simulation results indicate a small yet measurable change in coil impedance for the deep seated notch. Efforts are underway to verify simulations with measurements.

CONCLUSION

Multi-frequency EC coil measurements were presented for an air core pancake coil with 4 mm ID and 18 mm OD above a subsurface 2D notch located 9 mm deep in a 10 thick aluminium plate. Multi-frequency coil measurements for a subsurface notch in 15 mm thick aluminium plate at the test frequencies indicated the need for coil and test frequency optimization. 3D numerical simulations for coil optimization suggested larger coil ID (20 mm) and OD (46 mm) and, lower frequency of operation (140 Hz) for subsurface defects in thicker (15 mm) aluminium plate. Simulated coil impedance for the optimized parameters indicates small variation in coil impedance which could be detected using a highly sensitive receiver such as the Giant Magneto Resistive (GMR) sensor.

ACKNOWLEDGEMENT

The authors thank Prof V. Srinivas, Department of Physics, Indian Institute of Technology Madras for providing access to coil winding machine, and K. Sudhakar, K. Vishwanath, and J. L. Narasimha Murthy in the Department of Engineering Design, Indian Institute of Technology Madras for their extended help during experiments.

REFERENCES

1. Blitz, J., "Electrical and Magnetic Methods of Nondestructive Testing," Adam Hilger, Bristol, p.89-99 (1991).
2. Thollon, F. and Lebrun, B. and Burais, N. and Jayet, Y., "Numerical and experimental study of eddy current probes in NDT of structures with deep flaws," NDT&E Int., **28** (2), 97–102 (Apr. 1995).
3. Theodoulidis, T.P., Martinos, J,, and Poulakis, N., "Numerical results for the WFNDEC 2012 eddy current benchmark problem," (American Instittue of Physics, 1511, Melville, NY), **32**, 1825–1830 (2013).
4. Dodd, C. V. and Deeds, W. E., "Analytical Solutions to Eddy-Current Probe-Coil Problems," J. Appl. Phys., **39** (6), 2829 (1968).
5. Sikora, R., Chady, T., Gratkowski, S., Komorowski, M., and Stawicki, K., "Eddy Current Testing of Thick Aluminum Plates with Hidden Cracks," in *Review of Progress in Quantitative Nondestructive Evaluation*, eds. D. O. Thompson and D. E. Chimenti, (American Institute of Physics 657, Melville, NY) **22**, 427–434 (2003).